Targeting CD99 Compromises the Oncogenic Effects of the Chimera EWS–FLI1 by Inducing Reexpression of Zyxin and Inhibition of GLI1 Activity

Tommaso Balestra[1,2], Maria Cristina Manara[1], Maria Antonella Laginestra[1], Michela Pasello[1], Alessandra De Feo[1], Cristian Bassi[3], Clara Guerzoni[1], Lorena Landuzzi[1], Pier-Luigi Lollini[2], Davide Maria Donati[4,5], Massimo Negrini[3], Mauro Magnani[6], and Katia Scotlandi[1]

ABSTRACT

Ewing sarcoma, a highly aggressive pediatric tumor, is driven by EWS–FLI1, an oncogenic transcription factor that remodels the tumor genetic landscape. Epigenetic mechanisms play a pivotal role in Ewing sarcoma pathogenesis, and the therapeutic value of compounds targeting epigenetic pathways is being identified in preclinical models. Here, we showed that modulation of CD99, a cell surface molecule highly expressed in Ewing sarcoma cells, may alter transcriptional dysregulation in Ewing sarcoma through control of the zyxin–GLI1 axis. Zyxin is transcriptionally repressed, but GLI1 expression is maintained by EWS–FLI1. We demonstrated that targeting CD99 with antibodies, including the human diabody C7, or genetically inhibiting CD99 is sufficient to increase zyxin expression and induce its dynamic nuclear accumulation. Nuclear zyxin functionally affects GLI1, inhibiting targets such as NKX2–2, cyclin D1, and PTCH1 and upregulating GAS1, a tumor suppressor protein negatively regulated by SHH/GLI1 signaling. We used a battery of functional assays to demonstrate (i) the relationship between CD99/zyxin and tumor cell growth/migration and (ii) how CD99 deprivation from the Ewing sarcoma cell surface is sufficient to specifically affect the expression of some crucial EWS–FLI1 targets, both *in vitro* and *in vivo*, even in the presence of EWS–FLI1. This article reveals that the CD99/zyxin/GLI1 axis is promising therapeutic target for reducing Ewing sarcoma malignancy.

Introduction

Ewing sarcoma, the second most common bone malignancy in children, adolescents, and young adults (1) is genetically characterized by reciprocal chromosomal translocations that fuse an FET family gene with an ETS family gene, creating an aberrant transcription factor (1, 2). In most cases, the fusion transcript is represented by the hybrid EWS–FLI1 transcript, which drives broad epigenetic reprogramming, acting as a mediator of transcriptional hubs and producing higher transcriptional outputs than classical transcription factors (3–5). Aberrant expression of the chimera leads to deregulation of cell differentiation and increased cell proliferation, survival, and migration (5). As in most developmental cancers, additional recurrent mutations are rare in Ewing sarcoma (6, 7), indicating that substantial changes in the Ewing sarcoma transcriptome occur through fundamental epigenomic mechanisms rather than DNA alterations. Therefore, novel therapeutic approaches for Ewing sarcoma should consider targeting these epigenetic alterations. However, although emerging classes of small-molecule epigenetic drugs capable of manipulating the activity of chromatin-modifying enzymes are under active development (8), the genetic landscape of Ewing sarcoma is insufficiently understood for effective targeting and the management of patients with Ewing sarcoma is still based on conventional chemotherapeutic approaches. Patients with localized Ewing sarcoma have a survival rate of 70% to 80% thanks to intensive cytotoxic drug regimens (9). However, this intensive treatment is frequently associated with late effects. Furthermore, primary disseminated disease and relapse are associated with poor outcomes and specific novel treatment strategies are required to prevent metastasis formation.

The metastatic process in Ewing sarcoma cells is poorly understood. Metastasis can occur through various complementary and/or concomitant processes, including alteration of EWS–FLI1 protein levels (10) to promote the expression of stress-adaptive proteins or cell migration/survival effectors (1). Transcripts or proteins regulated by EWS–FLI1 include CD99 (11, 12), a cell membrane protein involved in many essential cellular functions, including cell adhesion and migration, cell death and differentiation, intracellular protein trafficking, endocytosis, and exocytosis (13, 14). Ewing sarcoma cells express high levels of CD99, which is required for the maintenance of Ewing sarcoma malignancy independent of the oncogenic driver EWS–FLI1. Ewing sarcoma cells deprived of CD99 but still expressing EWS–FLI1 showed dramatically inhibited growth, migration, and metastatic capabilities and tended to differentiate toward the neural lineage (12, 15, 16). Targeting CD99 either with specific antibodies (17–20), short hairpin RNA (shRNA) approaches (12, 16), and/or drugs such as clofarabine, which was found to act partially through CD99 (21), severely reduces cell proliferation and migration *in vitro* and tumor growth and metastasis formation *in vivo*, and is therefore a more feasible therapeutic approach than anti–EWS–FLI1 strategies. Notably, CD99 triggering has also been reported to induce actin

[1]Laboratory of Experimental Oncology, IRCCS Istituto Ortopedico Rizzoli, Bologna, Italy. [2]Department of Experimental, Diagnostic and Specialty Medicine (DIMES), University of Bologna, Bologna, Italy. [3]Department of Translational Medicine and for Romagna, and "Laboratorio per le Tecnologie delle Terapie Avanzate" (LTTA), University of Ferrara, Ferrara, Italy. [4]Clinica Ortopedica III, IRCCS Istituto Ortopedico Rizzoli, Bologna, Italy. [5]Department of Biomedical and Neuromotor Sciences (DIBINEM), University of Bologna, Bologna, Italy. [6]Department of Biomolecular Sciences, University of Urbino, Fano, Italy.

Note: Supplementary data for this article are available at Molecular Cancer Therapeutics Online (http://mct.aacrjournals.org/).

Corresponding Author: Katia Scotlandi, Laboratory of Experimental Oncology, IRCCS Istituto Ortopedico Rizzoli, via di Barbiano, 1/10, Bologna 40136, Italy. Phone: 3905-1636-6760; Fax: 3905-1636-6763; E-mail: katia.scotlandi@ior.it

Mol Cancer Ther 2022;21:58–69

doi: 10.1158/1535-7163.MCT-21-0189

repolymerization and upregulation of zyxin, a zinc-finger protein that was shown to play a role either in actin filament organization at focal adhesion and cell-to-cell contact (22, 23) or in transducing mechanical stimuli from the cell membrane to the nucleus (24). EWS–FLI1 transcriptionally represses zyxin and zyxin reexpression and was found to be sufficient to restore actin cytoskeletal integrity and inhibition of cell migration and metastasis to levels comparable with those observed after compromise of EWS–FLI1 oncogenic expression (25, 26). Here, we showed that targeting CD99 induced upregulation of zyxin and its recruitment to the nuclei, where it inhibited the activity of GLI1, a transcriptional factor with high expression in Ewing sarcoma because it is directly sustained by EWS–FLI1 and required for transformation (27). The results obtained with the human monospecific bivalent single-chain fragment variable diabody C7 (dAbd C7; refs. 17, 28) directed against CD99, where results were particularly clinically promising.

Materials and Methods

Cell lines and primary cultures

6647 and TC-71 cells were kindly provided by Timothy Triche, Jr (Children's Hospital, Los Angeles); SK-N-MC (ATCC, catalog No. CRL-2270, RRID:CVCL_1398), SK-ES-1 (CLS, catalog No. 300435/p738_SK-ES-1, RRID:CVCL_0627), and RD-ES (CLS, catalog No. 300410/p763_RD-ES, RRID:CVCL_2169) were purchased from the ATCC; IOR/CAR and LAP-35 cells (RRID:CVCL_A096) were previously established in our laboratory (18); and A673 cells (CLS, catalog No. 300454/p491_A-673, RRID:CVCL_0080) were provided by Heinrich Kovar (St. Anna Kinderkrebsforschung). PDX-EW#2-C cells and PDX-EW#4-C cells were established from the corresponding Ewing sarcoma patient-derived xenografts (PDX) after the first passage in animals as previously described (29). Human mesenchymal stem cells (MSC) were kindly provided by Enrico Lucarelli (Istituto Ortopedico Rizzoli) and cultured as previously described (11, 30). Ewing sarcoma cells were cultured in Iscove's modified Dulbecco's medium (IMDM; ECB2072L, EuroClone) supplemented with 10% FBS (ECS0180L, EuroClone), 100 U/mL penicillin, and 100 mg/mL streptomycin (P0781–100ML, Merck) and incubated at 37 °C in a humidified atmosphere containing 5% CO_2. All cell lines were tested for *mycoplasma* contamination (MycoAlert Mycoplasma Detection Kit, LT07–418, Lonza) before starting experiments and were authenticated by short tandem repeat (STR) PCR analysis using a PowerPlex ESX Fast System kit (DC1710, Promega; last control December 2019).

Stable and transient transfection and lentiviral infection

Stable CD99 silencing was achieved in TC-71 and IOR/CAR cells as previously described (12, 16). For transient zyxin silencing, cells were transfected with siRNA sequences targeting zyxin (ON-TARGETplus SMARTpool, FE5M01634010020, Dharmacon) or irrelevant targets (ON-TARGETplusFE5D0012061320, Dharmacon). Transfections were performed using TransIT-X2 (MIR 6000, Mirus) according to the manufacturer's protocol. Cells were used for *in vitro* assays after 48 hours. For forced overexpression of zyxin, 6647 and TC-71 cells were infected with the pMSCV–human zyxin (hZyxin) vector (kindly provided by Mary Catherine Beckerle, University of Utah, UT) or control pMSCV-empty vector (kindly provided by Bruno Calabretta, Thomas Jefferson University, PA), and were selected with puromycin (P8833, 500 ng/mL; Merck). Stable inducible CD99 silencing was achieved through sequential transfection of A673 cells with the plasmid pcDNA/6TR (Thermo Fisher Scientific), encoding the reverse tetracycline-responsive transcriptional activator and the plasmid pTER vector (kindly provided by Karine Laud-Duval, Institut Curie, Paris), and engineered in our laboratory to express CD99 shRNA. The cells were cultured in the absence of tetracycline and selected with blasticidin (R21001, 2 μg/mL) and zeocin (R250–01, 50 μg/mL), both purchased from Thermo Fisher Scientific. To induce silencing of CD99, A673p6TR/pTERshCD99 cells were treated for 48 hours with tetracycline (T7660, 50 μg/mL), which was subsequently removed to allow recovery of CD99 expression. All subsequent experiments on transfected cell lines were performed in tandem with Western blotting to assess overexpression or silencing of specific targets as a control.

Anti-CD99 antibody treatment

The hybridoma used to produce the murine anti-CD99 mAb 0662 was kindly provided by Alain Bernard (Unité INSERM 343, Hospital de l'Archet, Nice). The anti-CD99 human monospecific bivalent single-chain fragment variable dAbd C7 was produced by Diatheva srl. Two million cells were seeded in 100-mm dishes and, after 48 hours, were treated with mAb 0662 (3 μg/mL) or the dAbd C7 (200 μg/mL) for 1 to 3 hours before harvesting and processing for Western blotting or qPCR, as described in the information to follow. For the immunofluorescence (IF) assay, 2×10^5 cells were seeded on coverslips coated with fibronectin (F1141, 3 μg/cm^2; Merck) for 48 hours and treated with the anti-CD99 antibodies for 1 to 3 hours, fixed, and processed as described in the information to follow.

In vitro parameters of malignancy

Ten thousand cells (10,000/cm^2) were seeded to assess cell viability over 96 hours with trypan blue live cell stain (T8154, Merck). Anchorage-independent growth was evaluated in 0.33% agarose (50100, SeaPlaque; Lonza) with a 0.5% agarose underlay. The cell suspension (3,300 cells) were plated in a 60-mm dish in semisolid medium (10% FBS IMDM) and incubated at 37°C in a humidified 5% CO_2 atmosphere. Colonies with more than 50 cells were counted on all plates after 7 days, using an inverted microscope (magnification 40x). The migration ability of Ewing sarcoma cells was assessed using Transwell chambers (Corning) with 8-μm pore-size polycarbonate filters. A suspension of 1×10^5 cells in 10% FBS IMDM was seeded in triplicate in the upper compartments, and incubated for 18 hours at 37°C in a humidified 5% CO_2 atmosphere. The cells that migrated through the filter into the lower chamber were counted using an inverted microscope with a 20x objective (magnification 200x) after methanol fixation and Giemsa staining (32884, Merck). All experiments were performed in triplicate.

Luciferase reporter gene assay

GLI1 transcriptional activity was assessed by a luciferase assay using a pGL3–Basic luciferase construct containing 8x *GLI*-binding sites fused to a chicken lens crystalline promoter (31). Cells were seeded in standard medium in 24-well fibronectin (3 μg/cm^2; Merck)-coated plates (30,000 cells/well), subjected to modification of zyxin expression and then transfected with 250 ng of *GLI1* signal reporter (kindly provided by Aykut Uren, Georgetown University,) with Lipofectamine 2000 (11668019, Thermo Fisher Scientific). Luciferase activity was measured according to the manufacturer's protocol using a Dual-Glo Luciferase Assay System (E2920, Promega). The firefly luciferase signal was normalized to that of Renilla luciferase, the internal control. When indicated, cells were treated with anti-CD99 antibodies (see above) 3 hours before luciferase signal measurement.

Immunoblot analysis

Western blotting was performed according to standard protocols. Equivalent amounts of protein were separated by electrophoresis on a 4% to 15% resolving gel (Mini-PROTEAN TGX Stain-Free Protein Gels; Bio-Rad) and transferred to nitrocellulose membranes. Membranes were incubated overnight with anti-Zyxin (EPR4302, rabbit, ab109316; dilution 1:2 000; Abcam), anti-CD99 (12E7; mouse, sc-53148; dilution 1:2 000; Santa Cruz Biotechnology), anti-GLI1 (rabbit, ab217326; dilution 1:1,000; Abcam), anti-GAPDH (FL-335, rabbit, catalog No. sc-25778, RRID: AB_10167668, dilution 1:10,000; Santa Cruz Biotechnology), and anti-Lamin B (C-20, goat, catalog No. sc-6216, RRID: AB_648156, dilution 1:10,000; Santa Cruz Biotechnology) primary antibodies. Horseradish peroxidase (HRP)–conjugated donkey anti-rabbit (NA9340V), sheep anti-mouse (NA9310V) both purchased from antibodies (GE Healthcare) or anti-goat (catalog No. sc-2020, RRID: AB_631728sc-2020; Santa Cruz Biotechnology) secondary antibodies were used (diluition 1:10,000). Proteins were visualized with an enhanced chemiluminescence (ECL) Western Blotting Detection System (Euroclone).

Immunoprecipitation

Cells were lysed in a buffer containing 10 mmol/L Tris HCl (pH 7.4), 150 mmol/L NaCl, 1% Triton-X 100, 5 mmol/L EDTA, 1% Na-deoxycholate, 0.1% SDS, and protease inhibitors. Total cell lysates (500 μg) were incubated for 16 hours with Protein G-Plus agarose beads (Calbiochem) and 1.5 μg of the anti-zyxin mAb (EPR4302, rabbit, ab109316; dilution 1:2,000; Abcam). Immunoprecipitated proteins were analyzed by Western blotting.

Immunofluorescence

Cells were fixed with 4% paraformaldehyde, permeabilized with 0.15% Triton X-100 (Merck) in PBS and incubated with the anti-Zyxin antibody (EPR4302, rabbit, ab109316; dilution 1:100; Abcam). A FITC-conjugated swine anti-rabbit secondary antibody (F025, dilution 1:80; Dako) was used. TRITC-conjugated phalloidin (5 U/mL; P1951, Sigma) was applied for 30 minutes at room temperature to visualize actin filaments. Nuclei were counterstained with Hoechst 33258 (No. 861405, Merck). Images were acquired using a Nikon ECLIPSE 90i microscope and were then analyzed with NIS-Elements software (RRID: SCR_014329, Nikon).

Immunohistochemistry

An avidin–biotin–peroxidase method was used for immunostaining formalin-fixed, paraffin-embedded samples (Vector Laboratories) from dAbd C7 treated PDX-EW#2 tumors (29). Untreated PDX-EW#2 tumors were included as controls. Antigen retrieval was performed using citrate buffer (pH 6.0), prior to incubation with the anti-zyxin (EPR4302, rabbit, ab109316 dilution 1:100; Abcam). For CD99 evaluation, an anti-CD99 antibody (O13, mouse, No. MA5–12287; dilution 1:150; Thermo Fisher Scientific) was used without antigen retrieval.

RNA extraction and qPCR

Total RNA from snap-frozen tissue samples and cell lines was extracted with TRIzol reagent (No. 15596018, Thermo Fisher Scientific). Nucleic acid quality and quantity were assessed with a NanoDrop spectrophotometer (ThermoFisher Scientific). Total RNA of each sample was reverse-transcribed into cDNA using a High-Capacity cDNA Reverse Transcription Kit (ThermoFisher Scientific) according to the manufacturer's protocols. qPCR was performed on a ViiA7 system (ThermoFisher Scientific) using SYBR PCR Master Mix or TaqMan PCR Master Mix (Thermo Fisher Scientific). Predesigned TaqMan probes (ThermoFisher Scientific) for Zyxin (Hs00899658_m1), Cyclin D1 (CCND1; Hs00765553), and GAPDH (Hs99999905_m1) were used. The following primers were used: PATCHED1-forward, 5′-AATGGGTCCACGACAAAGCCGACTA-3′ and reverse, 5′-TCCCGCAAGCCGTTGAGGTAGAAAG-3; GAS1 forward, 5′-GAAGGGATGGTTGGGGATAC-3′ and reverse, 5′-TGCAGACGAGTTGGGAGTTTC-3; GAPDH forward, 5′-GAAGGT GAAGGTCGGAGTC-3′ and reverse, 5′-GAAGATGGTGATGGGATTTC-3′. mRNA expression levels were normalized to that of the housekeeping gene GAPDH, and the $2^{-\Delta\Delta Ct}$ method was used to compare the mRNA expression levels in the treated cells with those in untreated control cells (32).

Expression analysis of HEDGEHOG-GLI1 pathway-associated genes

We fused microarray data available in the laboratory to validate the regulation of *GLI1*-associated genes by CD99. Specifically, we employed data from biological duplicates of untreated cells (CTR), tetracycline-treated A673p6TR7shCD99cells, and A673p6TR7shCD99 cells with removal of tetracycline after 24/48 hours (tetracycline- 24/48 hours) using an Agilent whole human genome microarray (60,000 unique human transcripts, Agilent Technologies).

Raw data were analyzed with Feature Extraction 10.7.3.1 software, normalized using quantile normalization and $\log_2$ transformed with GeneSpring GX v.14.8 software (Agilent Technologies).

We performed gene set enrichment analysis sequencing (seqGSEA, RRID:SCR_005724; ref. 33) using the selected gene set PID_HEDGEHOG_GLI_PATHWAY (34) from the Molecular Signatures Database (MsigDB) and additional GLI pathway-related genes (35) as the gene set (Supplementary Table S1). Beginning with the whole $\log_2$ expression matrix, we investigated whether the above considered gene set was enriched in A673p6TR/shCD99 tetracycline or A673p6TR/shCD99 tetracycline- 24/48-hour cells. Specifically, the text entry option in GSEA software allowed us to create our custom gene set by entering the genes for PID_HEDGEHOG_GLI_PATHWAY (from the pathway interaction database; PID) and hedgehog signaling pathway genes reported in Skoda AM and colleagues (35). A heatmap of genes included in the core enrichment set was performed using the ComplexHeatmap R package (RRID:SCR_017270; ref. 36).

Normalized $\log_2$ expression values for the only genes included in the evaluated gene set were reported in Supplementary Table S2.

Statistical analyses

All statistical analyses were performed using Prism version 6.0 (RRID:SCR_005375; GraphPad Prism Software RRID:SCR_002798). Differences among means were evaluated by one-way ANOVA with Tukey multiple comparisons test, whereas a two-tailed Student *t* test was used for comparisons between two groups. Correlation analyses were performed using the Spearman correlation test. The differences with $P < 0.05$ were considered statistically significant.

Results

Zyxin is deregulated in aggressive Ewing sarcoma but reexpressed by targeting CD99

Previous observations indicated that zyxin is downregulated in Ewing sarcoma and repressed by EWS–FLI1 (26) and that zyxin gene transfer into *EWS/FLI1*–transformed fibroblasts elicits actin cytoskeletal reorganization, inhibition of anchorage-independent growth and cell migration, and impairment of tumor formation in athymic mice (25). Here, we extended these observations to a large panel of

patient-derived cell lines including novel cell lines established from PDXs (29). Most of the Ewing sarcoma cell lines had lower zyxin expression than MSCs (**Fig. 1A**; Supplementary Fig. S1A), which are considered the putative cells of origin of Ewing sarcoma (37). However, zyxin expression was heterogeneous among the Ewing sarcoma cell lines and zyxin expression levels inversely correlated with the migration ability of Ewing sarcoma cells (Spearman correlation test, $r = -0.85$; $P = 0.0061$; **Fig. 1B**). We used gain- and loss-of-function approaches to confirm this relationship. shRNA-mediated-silencing of zyxin in IOR/CAR cells, with relatively high zyxin expression (Supplementary Fig. S1B and S1C), promoted migration (**Fig. 1C**), while stable forced expression of zyxin in low-zyxin-expression 6647 and TC-71 cells (Supplementary Fig. S1B and S1C) inhibited migration (**Fig. 1C**). Similarly, gain- and loss-of-function modulation of zyxin resulted in cell-growth regulation under both standard (**Fig. 1D**) and anchorage-independent conditions (**Fig. 1E**), consistent with its previously reported tumor suppressor function in *EWS-FLI1*–transformed murine fibroblasts (25).

We thus further investigated the crosstalk between CD99 and zyxin based on a previous study (38) showing zyxin upregulation in response to CD99 triggering in the Ewing sarcoma cell line 6647. Silencing of CD99 (Supplementary Fig. S2A) or its engagement by specific antibodies, including the human dAbd C7, induced an increase in zyxin expression (**Fig. 2A** and **B**). This relationship was also dynamically confirmed via tetracycline on inducible silencing of CD99 in A673 cells– zyxin expression increased when CD99 ablation was induced but declined as CD99 expression was restored (**Fig. 2C**). We observed no significant variations in the zyxin mRNA levels under any of these experimental conditions (Supplementary Fig. S2B), indicating that CD99 modulation regulates zyxin expression primarily posttranscriptionally.

The CD99-dependent effects on zyxin expression were independent of EWS-FLI1, whose expression remain constant after CD99 modulation (**Fig. 2B** and **C**; Supplementary Fig. S2C). Notably, reexpression of zyxin in Ewing sarcoma cells altered their morphology: numerous actin filament bundles were observed throughout the cytoplasm of cells with CD99 modulation (Supplementary Fig. S3), these bundles were reminiscent of the stress fibers seen within normal fibroblasts but lost after transformation with EWS–FLI (25).

Zyxin accumulates in the nucleus of CD99-deprived Ewing sarcoma cells and decreases GLI1 activity

Zyxin can shuttle between focal adhesions/the cytoplasm and the nucleus and its localization to particular intracellular compartments regulates its functions (24). In Ewing sarcoma, zyxin was found prominently in the cytoplasm, weakly at cell adhesion junctions, and transiently in nuclei (25). Here, we showed significant accumulation of zyxin in Ewing sarcoma cell nuclei when CD99 was not present on the cell surface; this accumulation was induced either by CD99 silencing (**Fig. 2D** and **E**) or induction of CD99 internalization after its triggering with specific antibodies (ref. 39; **Fig. 3A** and **B**). Variations in nuclear zyxin expression were observed by both IF (**Fig. 2D**; **Fig. 3A**) and Western blotting after nucleocytoplasmic fractionation (**Fig. 2E**; **Fig. 3B**), consistent with the observation that upon cell stretching (Supplementary Fig. S3), zyxin started to accumulate in the nucleus within 10 to 30 minutes (24); the zyxin protein may affect the transcriptional machinery through interactions with several nuclear factors (40, 41). Among these factors, GLI1 attracted our attention because its expression is upregulated by chimeric EWS—FLI1 and necessary for Ewing sarcoma transformation (27). In addition, zyxin was found to affect SHH/GLI1 signaling in the neural tube by physically interacting with the transcription factor GLI1 (42). Here, in Ewing sarcoma cells, the amount of cytoplasmic GLI1 (if present) was clearly lower than that of nuclear GLI1 (**Fig. 2E**; **Fig. 3B**) and zyxin indeed interacted with GLI1, as shown by coimmunoprecipitation in 6647 cells treated (1–3 hours) or not treated with the anti-CD99 mAb 0662 (**Fig. 3C**).

Our luciferase reporter assay indicated that forced overexpression of zyxin in TC-71 Ewing sarcoma cells was sufficient to significantly decrease the activity of GLI transcription factors, while its silencing in IOR/CAR cells increased their activity (**Fig 4A**). Moreover, treatment of 6647 Ewing sarcoma cells with anti-CD99 antibodies for 3 hours functionally inhibited GLI transcription factors (**Fig. 4B**). Under all three experimental conditions, the GLI1 expression levels did not change (**Fig. 4A** and **B**). To further confirm that zyxin modulation specifically affects the transcriptional function of GLI1, we analyzed the expression of the GLI1 target genes *NKX2–2, Patched1 (PTCH1), CyclinD1 (CCND1)*, and *GAS1* after zyxin silencing or overexpression in 6647 cells by qPCR (**Fig. 4C**; Supplementary Fig. S4C). Zyxin ablation indeed increased the expression of the GLI1-upregulated targets *NKX2–2, PTCH1, CCND1* while decreasing that of *GAS1*, a tumor suppressor protein negatively regulated by SHH/GLI1 signaling (43), compared with that in control (SCR) cells(**Fig. 4C**, $P < 0.05$ Student *t* test). In contrast, zyxin overexpression led to the opposite changes in the expression levels of the selected *GLI1* targets (Supplementary Fig. S4C). Treatment with dAbd C7, which caused an increase in nuclear zyxin (**Fig. 3B**), accordingly led to decreased expression of the *GLI1*-upregulated targets *NKX2–2, PTCH1*, and *CCND1*, but increased expression of *GAS1* (**Fig. 4C**). These effects were abrogated by zyxin silencing (**Fig. 4C**), further supporting the specific action of zyxin in regulating Gli1 target expression.

To further validate the relationship among CD99, zyxin, and GLI1, we performed GSEA using PID_HEDGEHOG_GLI_PATHWAY (34) along with additional GLI-pathway–related genes (34, 35) as the gene set, assessing which phenotype between untreated A673p6TR7shCD99 cells (CTR), cells with tetracycline- 24/48 hours, and tetracycline-treated cells were enriched in the above considered gene set. Interestingly, GSEA showed that the expression profile of A673p6TR/pTERshCD99 tetracycline cells was negatively correlated with the genes implicated in GLI protein-mediated Hedgehog signaling (**Fig. 4D**), even if the evidence was not strong, in terms of the FDR. Specifically, among the core enriched genes, *NKX2–2* and cyclin expression were decreased in A673p6TR/pTERshCD99 tetracycline cells compared with A673p6TR/shCD99 TET- 24/48-hour cells (**Fig. 4E**). After tetracycline removal, CD99 reexpression led to an increase in the expression of genes included in the core enrichment set (Supplementary Table S3), suggesting the reactivation of GLI1 signaling (**Fig. 4E**). Modulation of some of these genes was also confirmed by qPCR (Supplementary Fig. S4D).

Functional inhibition of GLI1 by anti-CD99 treatment is maintained *in vivo*

PDXs are ideal models for testing therapeutic approaches. We already demonstrated the efficacy of the anti-CD99 dAbd C7 against PDX EW#2 alone and combined with irinotecan (29). Here, we took advantage of that experiment to demonstrate that the functional relationship among triggering of CD99, nuclear zyxin translocation, and GLI1 activity is also confirmed *in vivo*. The expression of CD99, zyxin, and selected *GLI1* targets was evaluated in two tumors per group of mice treated or not treated with the anti-CD99 dAbd C7 (**Fig. 5**). IHC evaluation of CD99 confirmed the absence of this adhesion molecule after treatment with the anti-CD99 antibody and the

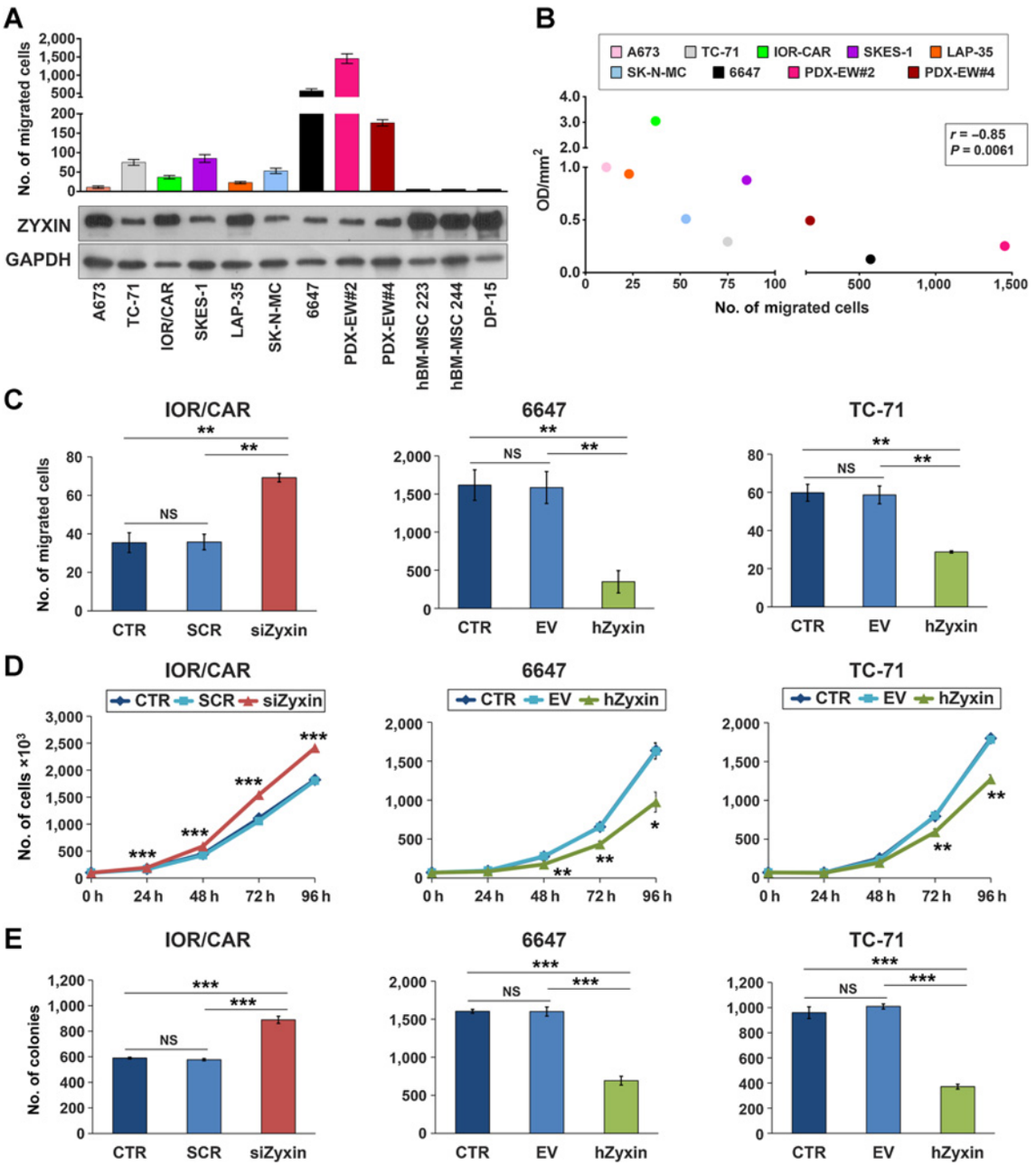

Figure 1.

Zyxin is deregulated and acts as a tumor suppressor in Ewing sarcoma cell lines. **A** and **B,** Analysis of cell migration and zyxin expression in a panel of human patient-derived cell lines and PDX-derived cell lines. Bone-marrow derived MSCs (hBM-MSCs) were used as normal controls. **A,** Top: the number of migrated cells is reported as the mean ± SE of three independent experiments. Bottom: representative Western blots of zyxin expression. GAPDH was used as a loading control. **B,** Migration data were correlated with densitometric analysis of zyxin expression. The ratio of adjusted volume optical density (OD/mm^2) of zyxin signal quantified against GAPDH. Correlation coefficient (r) and *P* value were calculated using Spearman rank test. **C–E,** IOR/CAR cells were transiently transfected with siRNA sequences targeting zyxin (siZyxin) or irrelevant target sequences (SCRs), while 6647 and TC-71 cells were stably transfected with hZyxin or empty vector (EV). Data represent the mean number of cells ± SE of three independent experiments. **C,** Effects of zyxin expression on cell migration; **, $P < 0.01$, one-way ANOVA. NS, not significant. **D,** Effects of of zyxin on cell growth in monolayer; *, $P < 0.05$; **, $P < 0.01$; ***, $P < 0.001$, Student t test versus untreated cells. h, hours. **E,** Effects of zyxin on cell growth in anchorage-independent conditions. ***, $P < 0.001$, one-way ANOVA.

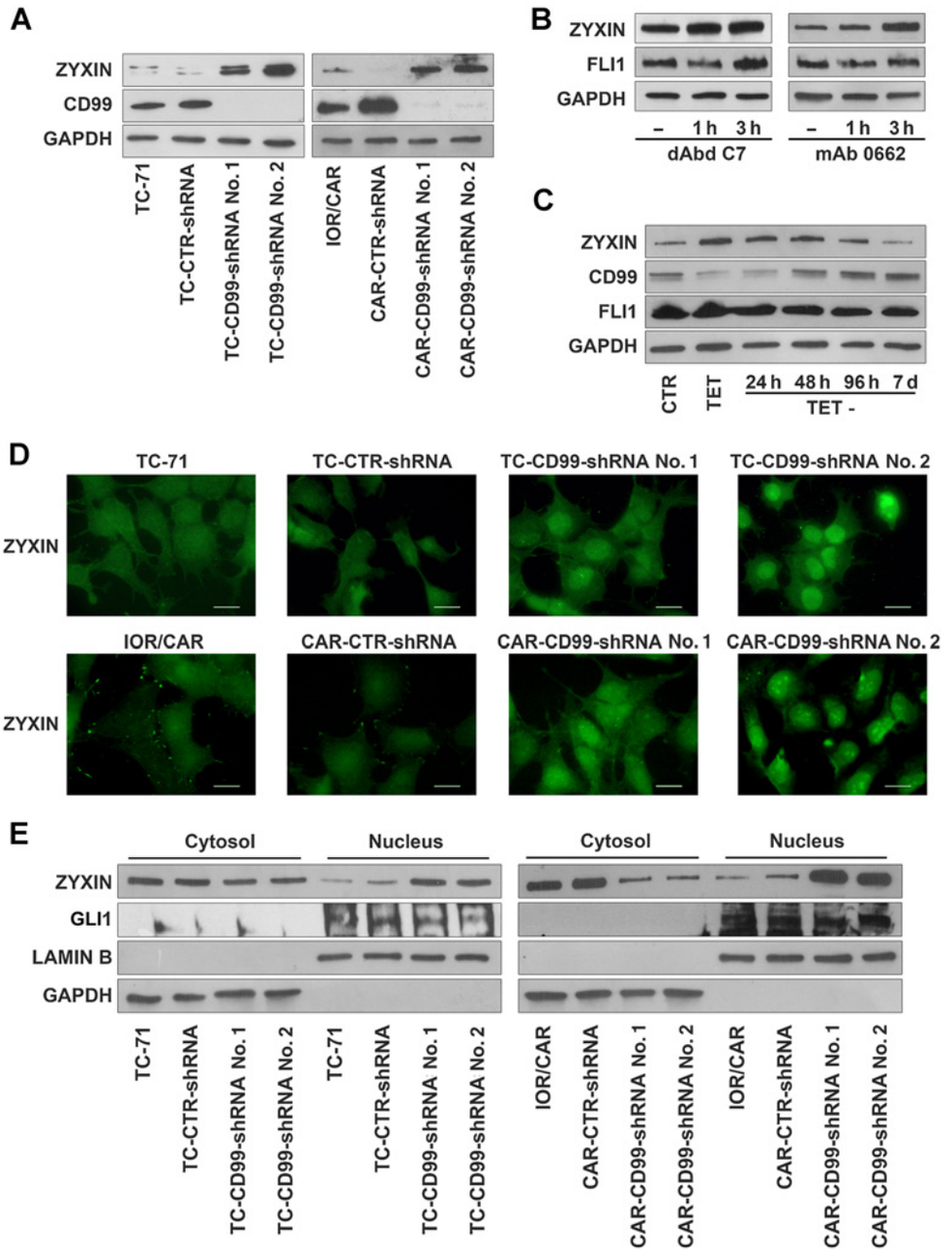

Figure 2.

CD99 loss of function promotes the increase of zyxin and induces zyxin nuclear localization. **A,** Western blotting of zyxin or CD99 after stable knock-down of CD99 in TC-71 and IOR/CAR (CD99-shRNA No. 1 and No. 2) compared with controls (CTR-shRNA). GAPDH was used as loading control. Blots are representative of 2 independent experiments. **B,** Western blotting of zyxin or FLI1 after treatment of 6647 cells with the anti-CD99 antibodies dAbd C7 (200 μg/mL) or mAb 0662 (3 μg/mL). GAPDH was used as loading control. Blots are representative of three independent experiments. **C,** The expression of zyxin, CD99, or EWS-FLI1 were evaluated by Western blotting in A673p6TR/pTERshCD99 cells treated with tetracycline (50 μg/mL) for 48 hours (TET) to induce CD99 silencing; subsequently, tetracycline was removed (TET-) to promote CD99 expression recovery. GAPDH was used as loading control. Blots are representative of 2 independent experiments. d, days. **D,** IF staining of zyxin after stable knock-down of CD99. Digital images are representative of at least 2 independent experiments and were taken using the image analysis software NIS-Elements (Nikon Italia); scale bar, 20 μm. **E,** Western blotting of zyxin or GLI1 in cytoplasmic versus nuclear cell fractions after stable knock-down of CD99. Lamin B and GAPDH were used as loading controls. Western blots are representative of 2 independent experiments.

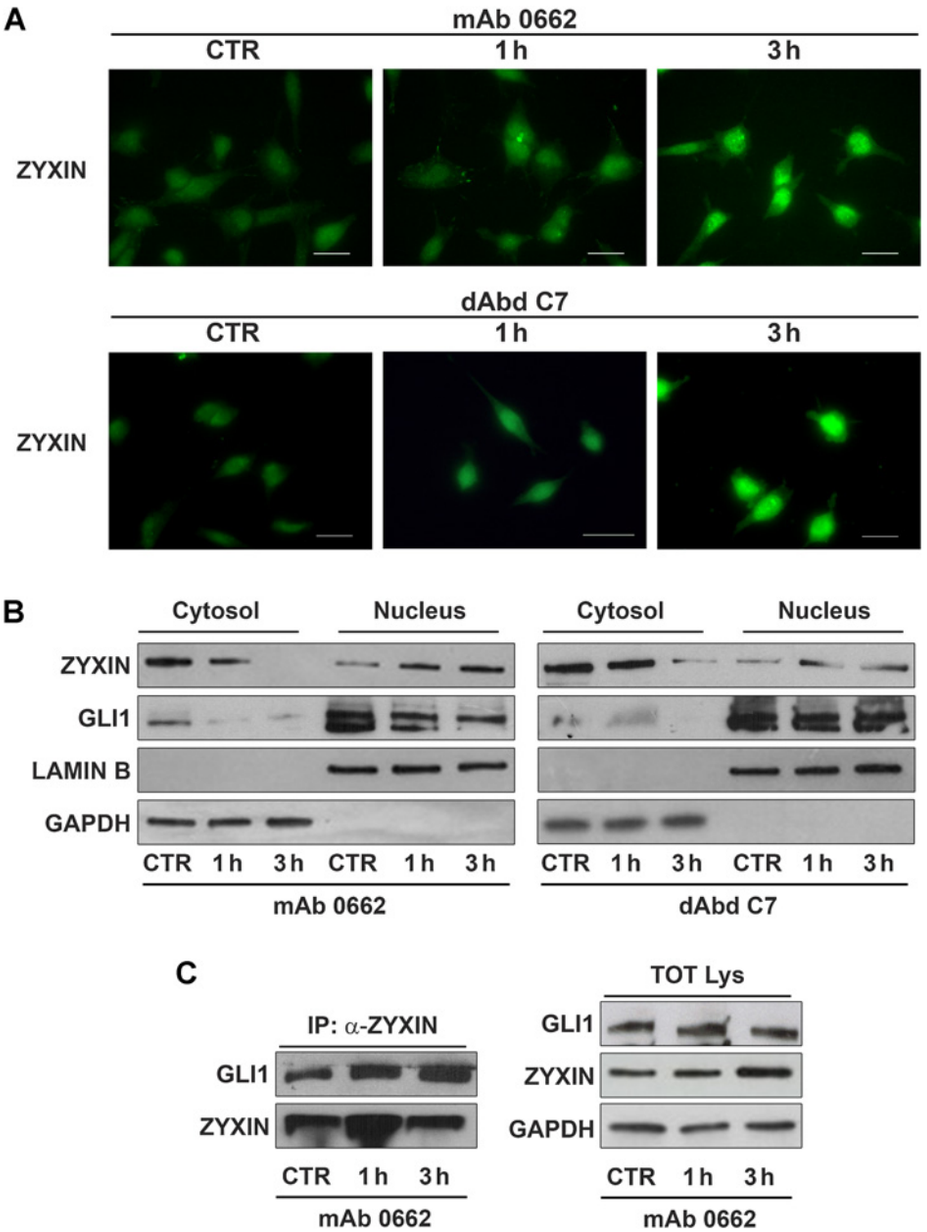

Figure 3.

Triggering of CD99 in 6647 cells induces dynamic accumulation of zyxin in the nucleus but does not affect GLI1 expression and localization. **A,** IF staining of zyxin. Digital images are representative of three independent experiments and were taken using the image analysis software NIS-Elements (Nikon Italia); scale bar, 20 μm. **B,** Western blotting of zyxin or GLI1 in cytoplasmic versus nuclear cell fractions. Lamin B and GAPDH were used as loading controls. Blots are representative of three independent experiments. **C,** Coimmunoprecipitation of zyxin and GLI1 in 6647 before and after treatment with 0662 mAb. Blots are representative of two independent experiments.

increased nuclear expression of zyxin (**Fig 5A**). In addition, we confirmed the significant downregulation of the GLI1 targets *NKX2–2, PTCH1*, and *CCND1* (**Fig 5B**). This finding further supports the potential value of CD99 antibodies as a therapeutic tool for Ewing sarcoma.

Discussion

Zyxin is a phosphoprotein implicated in actin cytoskeleton assembly and localized mainly at focal adhesions. Zyxin can, however, also shuttle between the cytoplasm and nucleus (44), where it may affect the transcriptional machinery (42, 44). In fact, besides the N-terminal domain mediating its association to focal adhesions (45), zyxin has a C-terminal LIM-domain comprising 3 zinc-finger motifs known to mediate protein–protein and/or protein–DNA interactions (46). Thus, zyxin is thought to act as a key interacting partner for diverse molecules, which allows it to execute a plethora of cellular functions and to play a dual oncogenic or tumor suppressive roles in cancer (47). In Ewing sarcoma, zyxin was reported to act as a tumor suppressor whose expression is repressed by the oncogenic driver EWS—FLI1. Reexpression of zyxin in Ewing sarcoma cells is sufficient to overcome the EWS—FLI1–induced alterations in actin cytoskeletal integrity and cell adhesion, inhibiting cell migration (25, 26). However, some tumor-suppressive properties of zyxin are thought to be independent of a physical interaction with the actin cytoskeleton. For example, the C-terminal region of zyxin contains three LIM domains able to interact with members of the cell cycle and apoptosis regulator protein (CRP) family (46), which are required for tumor cell death in response to retinoids and adriamycin (48), and with the tumor suppressor hWarts/LATS1, a serine threonine kinase that interacts with zyxin in dividing cells where it promotes cell exit from mitosis (49). In Ewing sarcoma,

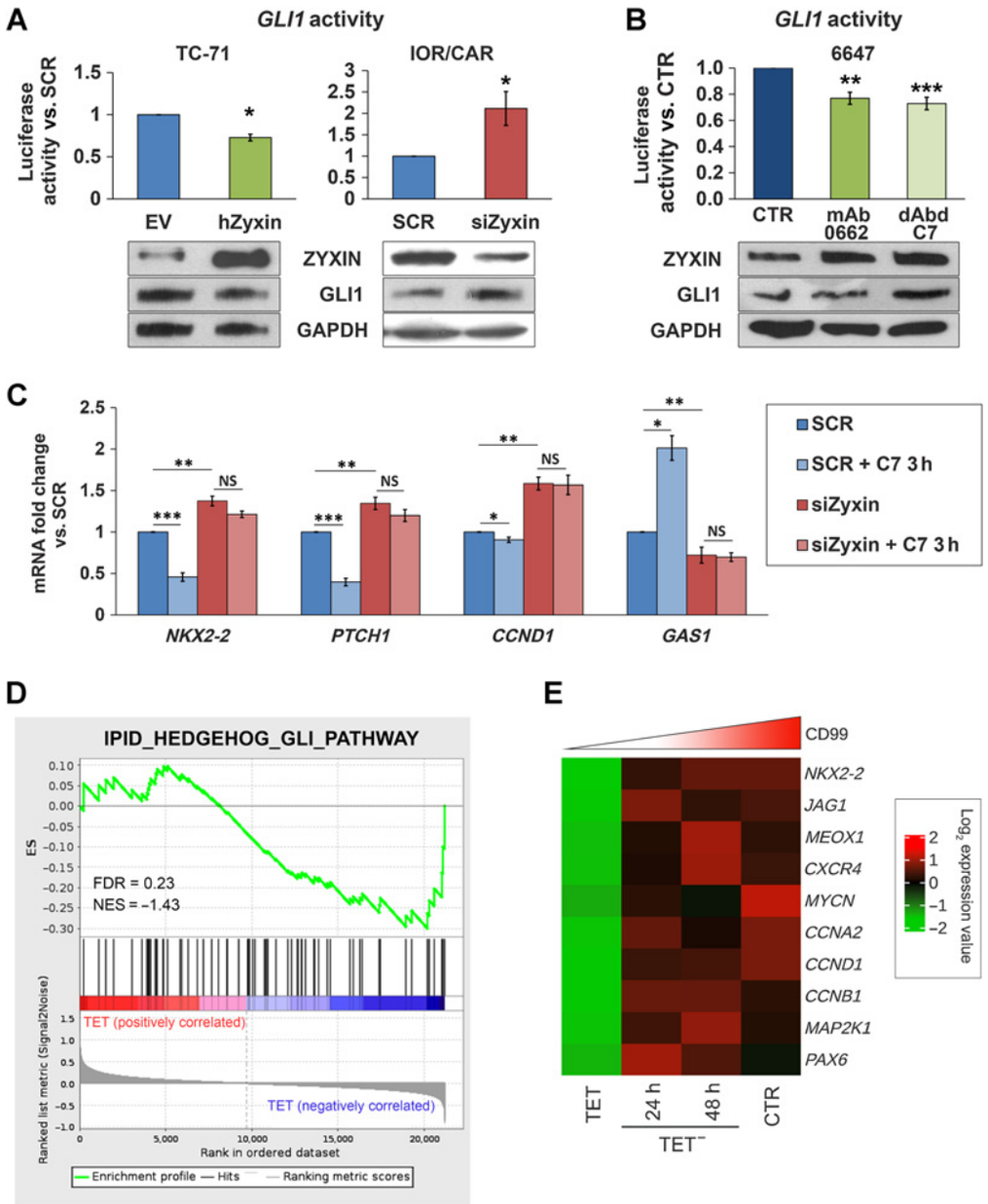

Figure 4.

Zyxin inhibits *GLI1* activity. **A** and **B,** Transcriptional activity of *GLI1* was evaluated by luciferase assay in cells modulated for zyxin expression. Top: data are shown as the ratio between the luciferase activity of EWS cells overexpressing zyxin (hZyxin) or silenced for zyxin (siZyxin) or modulated for zyxin after treatments with the anti-CD99 antibodies versus controls (EV, SCR, or CTR). Each column represents the mean ± SE of three independent experiments (*, $P < 0.05$; **, $P < 0.01$; ***, $P < 0.001$, Student *t* test). Bottom: Western blotting of a representative experiment to show zyxin or GLI1 expression in the different conditions. GAPDH was used as loading control. **C,** Relative expression of the GLI1 target genes *NKX2–2, PTCH1, CCND1*, and *GAS1* by qPCR. 6647 cells silenced or not (SCR) for zyxin (siZyxin) were treated or not with the anti-CD99 antibody dAbd C7 (200 μg/mL) for 3 hours. Data are shown as the mean ± SE of three independent experiments. (*, $P < 0.05$; **, $P < 0.01$; ***, $P < 0.001$, Student *t* test). **D,** GSEA was performed in A673p6TR7shCD99 treated with tetracycline (TET) with respect to cells after TET removal (TET-) using PID_HEDGEHOG_GLI_PATHWAY as gene set (33, 34). The enrichment score (ES) curve was obtained from GSEA software. In the enrichment plot, the x axis shows the rank order of genes. Vertical black line, position of the enriched genes (Hit) comprising the gene set. Bottom graph, ranked list metric (signal-to-noise ratio) for each gene as a function of the rank in the ordered dataset. NES, normalized enrichment scale. **E,** Heatmap of $\log_2$ expression value for core enrichment genes from GSEA.

we previously demonstrated the involvement of zyxin in proapoptotic pathways (38). Here, we furthered our research and demonstrated that cellular deprivation of CD99 induced the translocation and accumulation of zyxin in the nuclear compartment of Ewing sarcoma cells, where it may affect the transcriptional activity of GLI1. The mechanisms underlying the nucleocytoplasmic shuttling of zyxin are unclear but, at least in Ewing sarcoma, this process seems to be influenced by the presence or absence of CD99 on the cell surface. Similar to

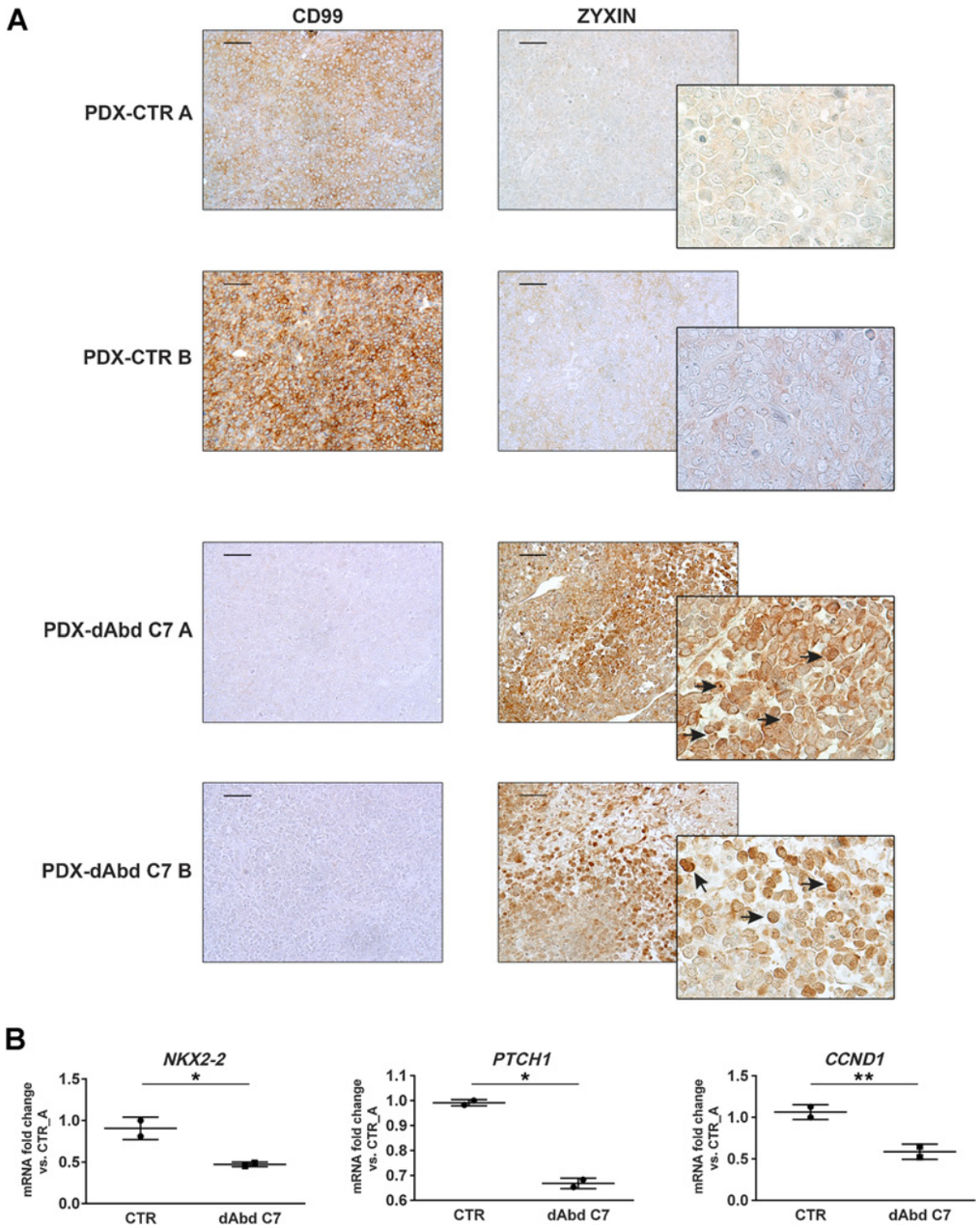

Figure 5.

Treatment of Ewing sarcoma xenografts with the anti-CD99 dAbd C7 increased the expression of zyxin and inhibited GLI1 transcriptional activity *in vivo*. **A,** IHC staining of CD99 and zyxin expression in two PDX-EW#2 samples treated or not (CTR) with the anti-CD99 dAbd C7 (29). Representative imagines are shown. Scale bar, 50 μm; 200x of magnification with zoomed insert to show details. **B,** qPCR analysis of the expression of the GLI1 target genes *NKX2-2, PTCH1* and *CCND1* in the same tumors treated or not treated with the anti-CD99 dAbd C7. Tumor samples were collected 72 hours after the end of the treatments. (*, $P < 0.05$; **, $P < 0.01$, Student *t* test).

observations in vascular smooth-muscle cells exposed to cyclic strain, within minutes after CD99 triggering, zyxin translocated from the cytoplasm to the nucleus of Ewing sarcoma cells. Application of mechanical stretch to cells was found to cause, in addition to cytoskeletal alterations, rapid nuclear accumulation of zyxin and modulation of the expression of various genes involved in the stretch response (24). During stress fiber assembly, zyxin was found to flow away from focal adhesions in synchrony with newly assembled actin bundles (50). Similar phenomena may have occurred in our models after modulation of CD99; its antibody binding induces actin polymerization (38). Future work is necessary to elucidate the mechanisms controlling the nuclear access and accumulation of zyxin. Whether the increase in nuclear zyxin expression results from conformational changes in the zyxin protein, enhancement of its nuclear import due

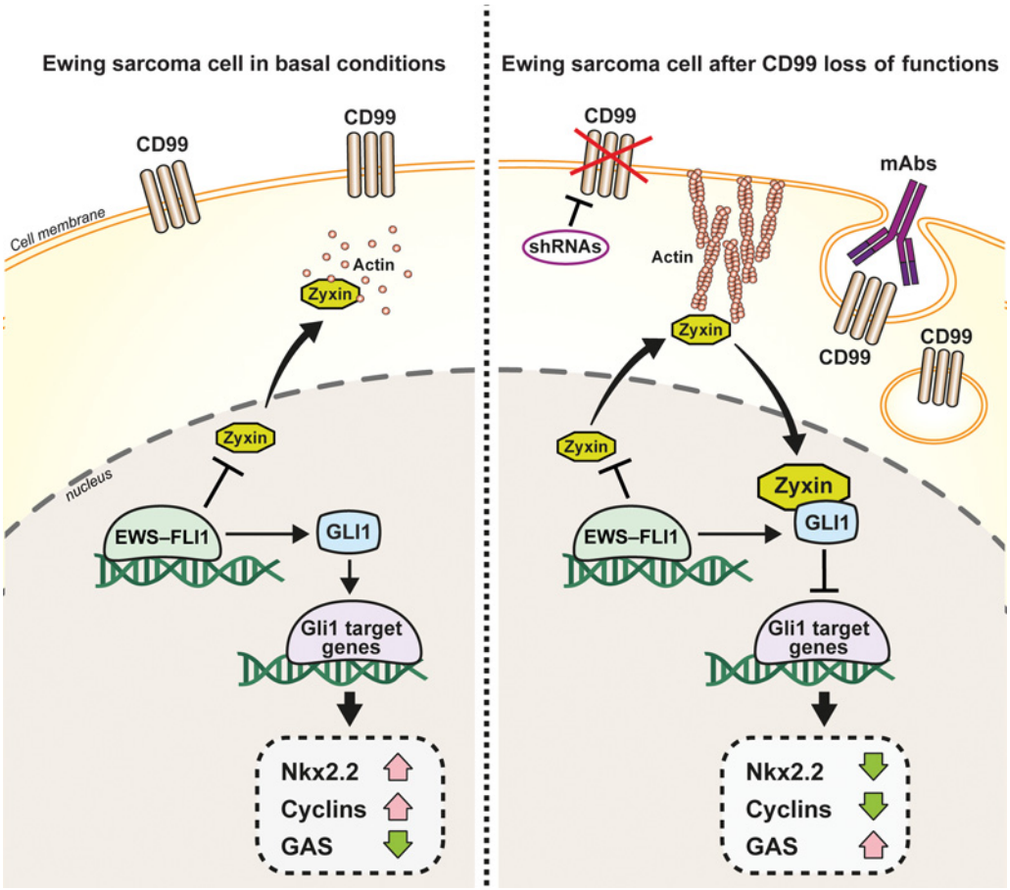

Figure 6.

Representation of the relationships between zyxin, CD99, GLI1, and EWS-FLI1 in EWS cells in basal condition or after CD99 loss of function. In basal condition, EWS-FLI1 downregulates zyxin; its expression is barely present in the cytoplasm of EWS cells, and upregulates GLI1 expression. After CD99 loss of function, zyxin translocates and accumulates in the nucleus where it directly interacts with GLI1 and inhibits its transcriptional functions.

to its interaction with other molecules, or specific inactivation of its nuclear export signal remains to be resolved and is beyond the scope of this study. Here, we highlight the therapeutic potential of nuclear recruitment of zyxin. Zyxin was found to interact with GLI1 and inhibit its transcriptional activity. This effect is particularly relevant in Ewing sarcoma, because GLI1 has been identified as direct transcriptional target of EWS—FLI1, and has been found to be essential in EWS—FLI1–induced signaling and required to sustain the malignant phenotype of Ewing sarcoma cells (27). EWS–FLI1 is overexpressed in patient-tumor specimens and Ewing sarcoma cell lines, and its targeting efficiently blocks Ewing sarcoma tumor growth (31). However, because GLI1 is activated by a noncanonical mechanism independent of SHH signaling, recently developed inhibitors of the G protein-coupled receptor Smoothened (SMO) are ineffective in this tumor. Ewing sarcoma indeed requires strategies that inhibit SHH signaling downstream of SMO or that can act directly in the nucleus to block GLI1 transcriptional activity. Here, we offer an alternative by using antibodies triggering CD99. Specifically, the human dAbd C7 is of potential therapeutic interest. dAbd C7 induces rapid and massive Ewing sarcoma cell death through MDM2 degradation and P53 reactivation and cooperates with doxorubicin to reduce tumor growth both *in vitro* and *in vivo* against Ewing sarcoma xenografts (18). Here, we showed that dAbd C7 is sufficient to increase zyxin expression and, more importantly, permits zyxin translocation to the nucleus where it functionally inhibits GLI1 both *in vitro* and *in vivo*. Downstream effects lead to modulation of GLI1 target genes such as *NKX2-2, CCND1, PTCH1* and *GAS*, which have been associated with cell growth maintenance, stemness, and cell migration (26). The molecular mechanisms activated by dAbd C7 are similar to those observed using the mouse mAb 0662, but dAbd C7, a small antibody, allows better tumor penetration than full-length mAbs and can be modified for affinity, stability, and blood clearance to improve efficacy; thus, it is a more promising treatment.

As summarized in **Fig. 6**, our results indicate that targeting CD99 not only delivers cell death signals, but also promotes the shuttling of zyxin to the nucleus where it can interact with the transcription factor GLI1 and repress expression of its targets. *GLI1* and *NKX2-2* are direct targets of EWS—FLI1 and are necessary for transformation (27, 33, 35). Therefore, we demonstrate that it is possible to interfere with EWS—FLI1–mediated effects using an antibody-based approach that targets a cell surface molecule that is constantly expressed at high levels in Ewing sarcoma cells.

Authors' Disclosures

T. Balestra reports grants from Associazione Italiana Ricerca sul Cancro (AIRC: ID. 18451 and ID. 22805); and other support from Onlus il Pensatore: Matteo Amitrano; Aurora Tomaselli, ricerca e prevenzione; Liberi di vivere, Luca Righi; Chiara Paradiso-la forza dell'amore onlus; and Associazione Mario Campanacci during the conduct of the study. M.C. Manara reports grants from AIRC (ID. 18451 and ID. 22805) during the conduct of the study. M.A. Laginestra reports grants from AIRC (ID. 18451 and ID. 22805) during the conduct of the study. M. Pasello reports grants from AIRC (ID. 18451 and ID. 22805) during the conduct of the study. A. De Feo reports grants from AIRC (ID. 18451 and ID. 22805) during the conduct of the study. C. Guerzoni reports grants from AIRC (ID. 18451 and ID. 22805) during the conduct of the study. L. Landuzzi reports grants from AIRC (ID. 18451 and ID. 22805) during the conduct of the study. D.M. Donati reports grants from AIRC (ID. 18451 and ID. 22805) during the conduct of the study, personal fees from Waldemar Link GmbH & Co., and personal fees from Zimmer GmbH outside the submitted work. M. Negrini reports grants from AIRC, Italian Ministry of Health, and grants from Horizon 2020 outside the submitted work. M. Magnani reports other support from Diatheva srl during the conduct of the study. K. Scotlandi reports grants from AIRC (ID. 18451 and ID. 22805) during the conduct of the study; in addition, K. Scotlandi has a patent 0001397621 licensed to Diatheva srl. No disclosures were reported by the other authors.

Authors' Contributions

T. Balestra: Conceptualization, data curation, formal analysis, investigation, visualization, writing–original draft, writing–review and editing. **M.C. Manara:** Investigation, writing–review and editing. **M.A. Laginestra:** Data curation, formal analysis, writing–review and editing. **M. Pasello:** Investigation, writing–review and editing. **A. De Feo:** Investigation, writing–review and editing. **C. Bassi:** Formal analysis, writing–review and editing. **C. Guerzoni:** Investigation, writing–review and editing. **L. Landuzzi:** Investigation, writing–review and editing. **P-L. Lollini:** Investigation, writing–review and editing. **D.M. Donati:** Supervision, writing–review and editing. **M. Negrini:** Resources, writing–review and editing. **M. Magnani:** Resources, writing–review and editing. **K. Scotlandi:** Conceptualization, resources, supervision, funding acquisition, writing–original draft, writing–review and editing.

Acknowledgments

We thank Cristina Ghinelli for the graphic support and the following associations for funding the PhD scholarship of T. Balestra: Onlus il Pensatore: Matteo Amitrano; Aurora Tomaselli, ricerca e prevenzione; Liberi di vivere, Luca Righi; Chiara Paradiso-la forza dell'amore onlus; Associazione Mario Campanacci.

The research leading to these results has received funding from AIRC under IG2016- ID. 18451 project – principal investigator (PI) K. Scotlandi and IG 2019 - ID. 22805 project – PI K. Scotlandi. The materials presented and views expressed here are the responsibility of the authors only. The sponsor takes no responsibility for any use made of the information set out.

The costs of publication of this article were defrayed in part by the payment of page charges. This article must therefore be hereby marked *advertisement* in accordance with 18 U.S.C. Section 1734 solely to indicate this fact.

Received March 2, 2021; revised July 30, 2021; accepted October 12, 2021; published first October 19, 2021.

References

1. Grunewald TGP, Cidre-Aranaz F, Surdez D, Tomazou EM, de Alava E, Kovar H, et al. Ewing sarcoma. Nat Rev Dis Primers 2018;4:5.
2. Delattre O, Zucman J, Plougastel B, Desmaze C, Melot T, Peter M, et al. Gene fusion with an ETS DNA-binding domain caused by chromosome translocation in human tumours. Nature 1992;359:162–5.
3. Riggi N, Knoechel B, Gillespie SM, Rheinbay E, Boulay G, Suva ML, et al. EWS-FLI1 utilizes divergent chromatin remodeling mechanisms to directly activate or repress enhancer elements in Ewing sarcoma. Cancer Cell 2014;26:668–81.
4. Sheffield NC, Pierron G, Klughammer J, Datlinger P, Schonegger A, Schuster M, et al. DNA methylation heterogeneity defines a disease spectrum in Ewing sarcoma. Nat Med 2017;23:386–95.
5. Scotlandi K. Biology of Ewing Sarcoma. Switzerland: Springer International Publishing; 2014. p.211–4.
6. Brohl AS, Solomon DA, Chang W, Wang J, Song Y, Sindiri S, et al. The genomic landscape of the Ewing Sarcoma family of tumors reveals recurrent STAG2 mutation. PLoS Genet 2014;10:e1004475.
7. Crompton BD, Stewart C, Taylor-Weiner A, Alexe G, Kurek KC, Calicchio ML, et al. The genomic landscape of pediatric Ewing sarcoma. Cancer Discov 2014;4:1326–41.
8. Pfister SX, Ashworth A. Marked for death: targeting epigenetic changes in cancer. Nat Rev Drug Discov 2017;16:241–63.
9. Gaspar N, Hawkins DS, Dirksen U, Lewis IJ, Ferrari S, Le Deley MC, et al. Ewing sarcoma: current management and future approaches through collaboration. J Clin Oncol 2015;33:3036–46.
10. Franzetti GA, Laud-Duval K, van der Ent W, Brisac A, Irondelle M, Aubert S, et al. Cell-to-cell heterogeneity of EWSR1-FLI1 activity determines proliferation/migration choices in Ewing sarcoma cells. Oncogene 2017;36:3505–14.
11. Amaral AT, Manara MC, Berghuis D, Ordonez JL, Biscuola M, Lopez-Garcia MA, et al. Characterization of human mesenchymal stem cells from ewing sarcoma patients. Pathogenetic implications. PLoS One 2014;9:e85814.
12. Rocchi A, Manara MC, Sciandra M, Zambelli D, Nardi F, Nicoletti G, et al. CD99 inhibits neural differentiation of human Ewing sarcoma cells and thereby contributes to oncogenesis. J Clin Invest 2010;120:668–80.
13. Manara MC, Pasello M, Scotlandi K. CD99: a cell surface protein with an oncojanus role in tumors. Genes (Basel) 2018;9:159.
14. Pasello M, Manara MC, Scotlandi K. CD99 at the crossroads of physiology and pathology. J Cell Commun Signal 2018;12:55–68.
15. Kreppel M, Aryee DN, Schaefer KL, Amann G, Kofler R, Poremba C, et al. Suppression of KCMF1 by constitutive high CD99 expression is involved in the migratory ability of Ewing's sarcoma cells. Oncogene 2006;25:2795–800.
16. Ventura S, Aryee DN, Felicetti F, De Feo A, Mancarella C, Manara MC, et al. CD99 regulates neural differentiation of Ewing sarcoma cells through miR-34a-Notch-mediated control of NF-kappaB signaling. Oncogene 2016;35:3944–54.
17. Gellini M, Ascione A, Flego M, Mallano A, Dupuis ML, Zamboni S, et al. Generation of human single-chain antibody to the CD99 cell surface determinant specifically recognizing Ewing's sarcoma tumor cells. Curr Pharm Biotechnol 2013;14:449–63.
18. Guerzoni C, Fiori V, Terracciano M, Manara MC, Moricoli D, Pasello M, et al. CD99 triggering in Ewing sarcoma delivers a lethal signal through p53 pathway reactivation and cooperates with doxorubicin. Clin Cancer Res 2015;21:146–56.
19. Scotlandi K, Baldini N, Cerisano V, Manara MC, Benini S, Serra M, et al. CD99 engagement: an effective therapeutic strategy for Ewing tumors. Cancer Res 2000;60:5134–42.
20. Scotlandi K, Perdichizzi S, Bernard G, Nicoletti G, Nanni P, Lollini PL, et al. Targeting CD99 in association with doxorubicin: an effective combined treatment for Ewing's sarcoma. Eur J Cancer 2006;42:91–6.
21. Celik H, Sciandra M, Flashner B, Gelmez E, Kayraklioglu N, Allegakoen DV, et al. Clofarabine inhibits Ewing sarcoma growth through a novel molecular mechanism involving direct binding to CD99. Oncogene 2018;37:2181–96.
22. Guo WH, Wang YL. Retrograde fluxes of focal adhesion proteins in response to cell migration and mechanical signals. Mol Biol Cell 2007;18:4519–27.
23. Ngu H, Feng Y, Lu L, Oswald SJ, Longmore GD, Yin FC. Effect of focal adhesion proteins on endothelial cell adhesion, motility and orientation response to cyclic strain. Ann Biomed Eng 2010;38:208–22.
24. Cattaruzza M, Lattrich C, Hecker M. Focal adhesion protein zyxin is a mechanosensitive modulator of gene expression in vascular smooth muscle cells. Hypertension 2004;43:726–30.
25. Amsellem V, Kryszke MH, Hervy M, Subra F, Athman R, Leh H, et al. The actin cytoskeleton-associated protein zyxin acts as a tumor suppressor in Ewing tumor cells. Exp Cell Res 2005;304:443–56.
26. Fadul J, Bell R, Hoffman LM, Beckerle MC, Engel ME, Lessnick SL. EWS/FLI utilizes NKX2–2 to repress mesenchymal features of Ewing sarcoma. Genes Cancer 2015;6:129–43.
27. Beauchamp E, Bulut G, Abaan O, Chen K, Merchant A, Matsui W, et al. GLI1 is a direct transcriptional target of EWS-FLI1 oncoprotein. J Biol Chem 2009;284:9074–82.
28. Moricoli D, Muller WA, Carbonella DC, Balducci MC, Dominici S, Watson R, et al. Blocking monocyte transmigration in in vitro system by a human antibody scFv anti-CD99. Efficient large scale purification from periplasmic inclusion bodies in E. coli expression system. J Immunol Methods 2014;408:35–45.

29. Nanni P, Landuzzi L, Manara MC, Righi A, Nicoletti G, Cristalli C, et al. Bone sarcoma patient-derived xenografts are faithful and stable preclinical models for molecular and therapeutic investigations. Sci Rep 2019;9:12174.
30. Sciandra M, Marino MT, Manara MC, Guerzoni C, Grano M, Oranger A, et al. CD99 drives terminal differentiation of osteosarcoma cells by acting as a spatial regulator of ERK 1/2. J Bone Miner Res 2014;29:1295–309.
31. Beauchamp EM, Ringer L, Bulut G, Sajwan KP, Hall MD, Lee YC, et al. Arsenic trioxide inhibits human cancer cell growth and tumor development in mice by blocking Hedgehog/GLI pathway. J Clin Invest 2011;121:148–60.
32. Livak KJ, Schmittgen TD. Analysis of relative gene expression data using real-time quantitative PCR and the 2(-Delta Delta C(T)) Method. Methods 2001;25:402–8.
33. Subramanian A, Tamayo P, Mootha VK, Mukherjee S, Ebert BL, Gillette MA, et al. Gene set enrichment analysis: a knowledge-based approach for interpreting genome-wide expression profiles. Proc Natl Acad Sci U S A 2005;102:15545–50.
34. Schaefer CF, Anthony K, Krupa S, Buchoff J, Day M, Hannay T, et al. PID: the Pathway Interaction Database. Nucleic Acids Res 2009;37:D674–9.
35. Skoda AM, Simovic D, Karin V, Kardum V, Vranic S, Serman L. The role of the Hedgehog signaling pathway in cancer: a comprehensive review. Bosn J Basic Med Sci 2018;18:8–20.
36. Gu Z, Eils R, Schlesner M. Complex heatmaps reveal patterns and correlations in multidimensional genomic data. Bioinformatics 2016;32:2847–9.
37. Tirode F, Laud-Duval K, Prieur A, Delorme B, Charbord P, Delattre O. Mesenchymal stem cell features of Ewing tumors. Cancer Cell 2007;11:421–9.
38. Cerisano V, Aalto Y, Perdichizzi S, Bernard G, Manara MC, Benini S, et al. Molecular mechanisms of CD99-induced caspase-independent cell death and cell-cell adhesion in Ewing's sarcoma cells: actin and zyxin as key intracellular mediators. Oncogene 2004;23:5664–74.
39. Manara MC, Terracciano M, Mancarella C, Sciandra M, Guerzoni C, Pasello M, et al. CD99 triggering induces methuosis of Ewing sarcoma cells through IGF-1R/RAS/Rac1 signaling. Oncotarget 2016;7:79925–42.
40. Crone J, Glas C, Schultheiss K, Moehlenbrink J, Krieghoff-Henning E, Hofmann TG. Zyxin is a critical regulator of the apoptotic HIPK2-p53 signaling axis. Cancer Res 2011;71:2350–9.
41. Kato T, Muraski J, Chen Y, Tsujita Y, Wall J, Glembotski CC, et al. Atrial natriuretic peptide promotes cardiomyocyte survival by cGMP-dependent nuclear accumulation of zyxin and Akt. J Clin Invest 2005;115:2716–30.
42. Martynova NY, Ermolina LV, Ermakova GV, Eroshkin FM, Gyoeva FK, Baturina NS, et al. The cytoskeletal protein Zyxin inhibits Shh signaling during the CNS patterning in Xenopus laevis through interaction with the transcription factor Gli1. Dev Biol 2013;380:37–48.
43. Seppala M, Depew MJ, Martinelli DC, Fan CM, Sharpe PT, Cobourne MT. Gas1 is a modifier for holoprosencephaly and genetically interacts with sonic hedgehog. J Clin Invest 2007;117:1575–84.
44. Nix DA, Beckerle MC. Nuclear-cytoplasmic shuttling of the focal contact protein, zyxin: a potential mechanism for communication between sites of cell adhesion and the nucleus. J Cell Biol 1997;138:1139–47.
45. Crawford AW, Michelsen JW, Beckerle MC. An interaction between zyxin and alpha-actinin. J Cell Biol 1992;116:1381–93.
46. Sadler I, Crawford AW, Michelsen JW, Beckerle MC. Zyxin and cCRP: two interactive LIM domain proteins associated with the cytoskeleton. J Cell Biol 1992;119:1573–87.
47. Kotb A, Hyndman ME, Patel TR. The role of zyxin in regulation of malignancies. Heliyon 2018;4:e00695.
48. Rishi AK, Zhang L, Boyanapalli M, Wali A, Mohammad RM, Yu Y, et al. Identification and characterization of a cell cycle and apoptosis regulatory protein-1 as a novel mediator of apoptosis signaling by retinoid CD437. J Biol Chem 2003;278:33422–35.
49. Hirota T, Morisaki T, Nishiyama Y, Marumoto T, Tada K, Hara T, et al. Zyxin, a regulator of actin filament assembly, targets the mitotic apparatus by interacting with h-warts/LATS1 tumor suppressor. J Cell Biol 2000;149:1073–86.
50. Smith MA, Hoffman LM, Beckerle MC. LIM proteins in actin cytoskeleton mechanoresponse. Trends Cell Biol 2014;24:575–83.